Internal structure of ultralow-crosslinked microgels: From uniform deswelling to phase separation

Michael Tennenbaum,[1] Caleb Anderson,[2] John S. Hyatt,[2,*] Changwoo Do,[3] and Alberto Fernandez-Nieves [1,2,4]

[1]*Department of Condensed Matter Physics, University of Barcelona, 08028 Barcelona, Spain*
[2]*School of Physics, Georgia Institute of Technology, Atlanta, Georgia 30332, USA*
[3]*Neutron Scattering Division, Oak Ridge National Laboratory, Oak Ridge, Tennessee 37831, USA*
[4]*ICREA-Institucio Catalana de Recerca i Estudis Avancats, 08010 Barcelona, Spain*

We perform small angle neutron scattering on ultralow-crosslinked microgels and find that while in certain conditions both the particle size and the characteristic internal length scale change in unison, in other instances this is not the case. We show that nonuniform deswelling depends not only on particle size, but also on the particular way the various contributions to the free energy combine to result in a given size. Only when polymer-solvent demixing strongly competes with ionic or electrostatic effects do we observe nonuniform behavior, reflecting internal microphase separation. The results do not appreciably depend on particle number density; even in concentrated suspensions, we find that at relatively low temperature, where demixing is not very strong, the deswelling behavior is uniform, and that only at sufficiently high temperature, where demixing is very strong, does the microgel structure change akin to internal microphase separation.

I. INTRODUCTION

Gels and in particular microgels have long been studied because of their ability to change size. This changing size can be controlled through a variety of means depending on the chemistry of the microgel. These means include temperature, pH, and salt concentration [1], as well as volume fraction [2–5]. Many common microgels are comprised of poly-*N*-isopropylacrylamide (PNiPAM), which is thermosenstive. Temperature in this case favors a demixing transition with the solvent above the so-called lower critical solution temperature (LCST). Random copolymerization with other monomers results in additional means to change the particle size. Adding acrylic acid (AAc), for example, enables charging of the polymer network at sufficiently high pH, bringing about electrostatic and ionic effects that greatly contribute to swelling equilibrium. Salt concentration, in this case, naturally becomes a third variable with which to tune the particle size.

Hence, in the case of ionic gels or microgels, temperature, pH, and salt concentration can all be used as a means to achieve size changes. Interestingly, for the case of microgels, the suspension volume fraction ϕ also provides a way to achieve this. In this case, ion-induced deswelling [2,4,6] and steric efffects [5,7,8], both of which can be relevant at sufficiently high ϕ, can force the particles into sizes that are smaller than their dilute size. In fact, it is the compressibility of microgels that renders them distinct from other deformable particles like emulsion droplets, which are effectively incompressible and can change shape only at constant volume. This compressibility results in significant difficulties for quantifying the volume fraction of microgel suspensions at sufficiently high particle number densities. It is thus common to introduce a generalized volume fraction ζ, which is defined in terms of the dilute microgel size. While $0 < \phi < 1$, ζ can take values larger than 1, indicating that in this limit, the microgels must interpenetrate, deform, and/or compress. It is in this way that ζ then becomes a potential means to also change the particle size.

In most common instances, these size changes are uniform throughout the microgel: All characteristic length scales change in unison. However, there are instances where this is no longer the case. For example, ultralow-crosslinked (ULC) microgels based on the copolymerization of PNiPAM and AAc in the absence of exogeneous crosslinker have been shown to exhibit nonuniform behavior through their deswelling transition with temperature at high pH [9]. This remarkable behavior was attributed to an internal microphase separation resulting from the competition between the electrostatic and ionic contribution to the free energy, which favors a swollen state, and demixing, which favors deswelling. As the temperature increases, the microgel particle deswells, but this deswelling, provided the polymer network is charged, causes both the Donnan potential and the ion concentration to increase, eventually causing the uniform shrinking of the microgel to become nonuniform due to internal microphase separation. However, whether such behavior can be attained by reaching a sufficiently small microgel size, but through different combinations of external parameters, remains to be explored.

Here we show that the specific conditions resulting in deswelling do indeed matter, confirming the internal microphase separation scenario where competing electrostatic/ionic effects and demixing all conspire to cause the

---

*Present address: Computational and Information Sciences Directorate, CCDC Army Research Laboratory, Aberdeen Proving Ground, MD 21005, USA.

022614-1

internal structural changes. We do this by shrinking the particles to similar sizes via two distinct pathways. In one pathway, we start from a swollen state, where the microgel is charged and is well mixed with the solvent, and reach a deswollen state by increasing salt concentration at constant pH and temperature. In the second pathway, we move from the same initial state to a comparable deswollen state in terms of size, but reached via increasing temperature at constant pH and salt concentration. The small angle neutron scattering (SANS) data are markedly different in either case; while in the first pathway, the scattered intensity monotonically decreases with the magnitude of the scattering wave vector q, in the latter, it exhibits a pronounced peak. In either case, we show that the characteristic internal length scale changes either in unison with the size, reflecting uniform deswelling, or reflects internal microphase separation, reflecting nonuniform behavior. Increasing ζ does not appreciably change our findings for dilute suspensions, confirming that it is demixing and its competition with electrostatic and ionic contributions to the free energy what enables internal microphase separation. Overall, our results illustrate that depending on how a given microgel is deswollen, assuming uniform behavior might be a gross oversimplification relative to how the actual internal structure might change.

The rest of the paper is organized as follows. We start by describing our ULC microgels in Sec. II, focusing on their swelling behavior. We show that the size of the particles can be changed by either temperature, pH, or salt concentration, and that similar deswollen states can be reached by changing different combinations of these parameters. We then discuss SANS in Sec. III, focusing on data analysis. Section IV summarizes our findings, which include data for dilute suspensions at temperatures where the microgel behavior is uniform or characterized by internal microphase separation, as well as data for concentrated samples at different temperatures. Finally, we end by summarizing our results and presenting our conclusions.

II. ULTRALOW-CROSSLINKED MICROGELS

ULC microgels are known to exhibit rich behavior across their swelling and deswelling transition [9]. They are comprised of NiPAM and AAc and do not contain exogenous crosslinker; they only have a small number of self-crosslinks that arise during the polymerization reaction [10,11], justifying the "ultralow" part in the name used to refer to them. Their synthesis has been described elsewhere [9,10,12–14] and is similar to that used for generating crosslinked PNiPAM/AAc microgels possessing a rather homogeneous distribution of the AAc groups within the particles [15]. Our ULC microgels consist of 95% NiPAM and 5% AAc.

To measure the size of the particles we use dynamic light scattering (DLS). In these experiments, we determine the correlation function of the scattered intensity at a fixed scattering angle θ. The angle determines the magnitude of the scattering wave vector, $q = 4\pi n_s \sin(\theta/2)/\lambda_0$, with n_s the index of refraction of the solvent and λ_0 the wavelength of the incident beam. From the intensity autocorrelation function $g_2(q, \tau)$, with τ the correlation time, using the Siegert relation, we calculate the electric field correlation function $g_1(q, \tau)$,

which we then use to determine the diffusion coefficient D of the particles, since $g_1(q, \tau) \sim \exp[-\Gamma\tau]$, with $\Gamma = Dq^2$. From D, we can further obtain the hydrodynamic radius R_H of diffusing particles via the Stokes-Einstein equation: $R_H = k_B T/(6\pi \eta_s D)$, with k_B the Boltzmann constant, T the temperature, and η_s the solvent viscosity. Note that despite microgels are, to a large extent, comprised of solvent, particularly when swollen, we can nevertheless use the Stokes-Einstein equation with great accuracy since microgels are hydrodynamically opaque [16,17].

PNiPAM is temperature sensitive and has a LCST a little above room temperature. It mixes with water at low temperatures and demixes at temperatures $T > T_{LCST}$. Hence, PNiPAM microgels deswell with increasing temperature. This behavior, however, depends on pH, since our ULC microgels contain AAc. We emphasize that the presence of comonomers, including neutral AAc, has also been observed to interfere with the demixing process of PNiPAM [18]. However, because the amount of AAc in our microgels is small, we can assume all PNiPAM will demix at high T. In this case, for low pH, where the AAc is uncharged, the behavior is similar to that of PNiPAM-only microgels; see squares in Fig. 1(a). At pH values close to the pK_a of AAc, which is $\approx$4.4 for isolated AAc groups, the deswelling transition broadens; the particles ultimately reach the deswollen size obtained at lower pH, but this happens more gradually and at a larger temperature, as shown with circles in Fig. 1(a). In this case, the charged network results in a Donnan potential that attracts counterions; these raise the osmotic pressure inside the microgel contributing towards swelling, which then competes with the demixing favored by increasing temperature. This effect is more pronounced at even higher pH, where nearly all of the AAc groups in the microgel are ionized; see triangles in Fig. 1(a). In this case, even at $T \approx 60\,^\circ\text{C}$, the microgels are not fully deswollen.

The interplay between temperature and pH can also be seen by plotting the microgel size as a function of pH at constant temperature. While at high T, where demixing with the solvent is maximal, increasing pH causes only a mild increase in size from pH $\approx$6 [see triangles in Fig. 1(b)], at low T, where PNiPAM mixes with the solvent, the particles are already swollen at low pH and continuously swell up to pH $\approx$6, where they reach their maximum size [see squares in Fig. 1(b)]. At intermediate temperatures, the behavior nicely interpolates between these two; the particles are deswollen up to pH $\approx$5, and progressively swell to reach the maximum swelling state at pH $\approx$8; see circles in Fig. 1(b).

Another important quantity for microgel suspensions is the suspension viscosity η, which has been previously measured for the ULC microgels under consideration [10]. The importance of η relies on the fact that it can be used to obtain ζ and perhaps even more importantly, the collapsed size of the microgels. Note we use the term collapsed size to refer to the dry, solvent-free, state of the particles. The key to this connection comes from knowing that colloidal suspensions in the dilute regime have a viscosity that depends, via the Einstein-Batchelor equation [19–21], on the volume fraction ϕ. A measurement of $\eta = \eta(c)$, with c the weight concentration of the suspension, and a fit of the result to the Einstein-Batchelor equation, considering that $\phi = k\,c$, with k
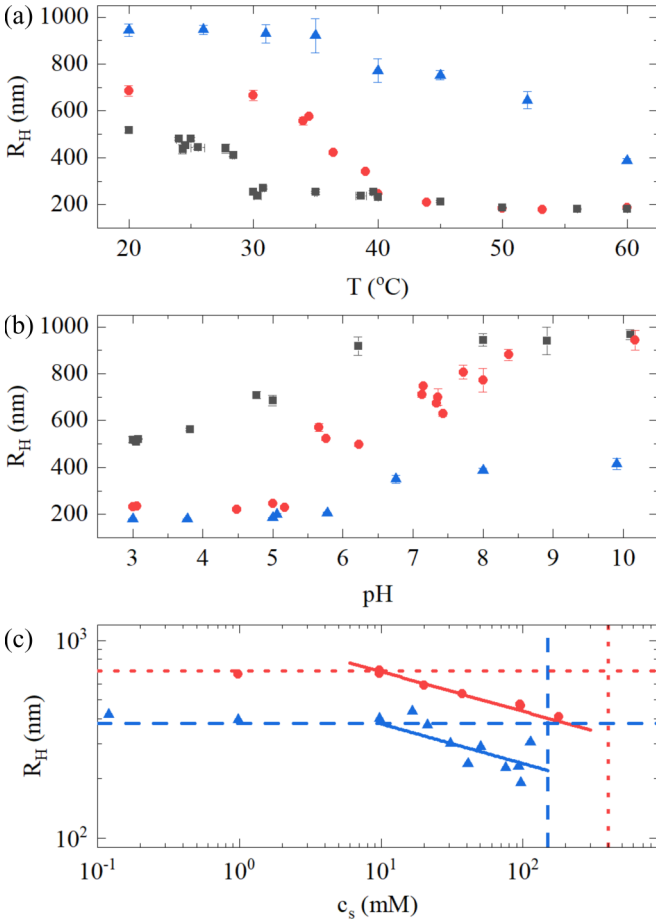
FIG. 1. (a) Hydrodynamic radius versus temperature at pH = 3 (squares), pH = 5 (circles), and pH = 8 (triangles). (b) Hydrodynamic radius versus pH with no added salt and $T = 20\,°C$ (squares), $T = 40\,°C$ (circles), and $T = 60\,°C$ (triangles). (c) Hydrodynamic radius versus salt concentration at pH = 8.5 ± 0.5 and $T = 40\,°C$ (circles) and $T = 60\,°C$ (triangles). The vertical lines (dashed for $T = 60\,°C$ and dotted for $T = 40\,°C$) demarcate where we begin to see aggregation and can no longer measure an individual particle size. The horizontal lines (dashed for $T = 60\,°C$ and dotted for $T = 40\,°C$) demarcate the dilute size without salt for the same pH and temperature. The solid lines correspond to power laws with exponent $-1/5$.

a constant, naturally provides k. The resultant value of k can then be used to determine $\zeta = k\,c$, even in the concentrated regime. Recall, however, that in this case, $\zeta \neq \phi$: While the volume fraction ϕ depends on the actual particle volume, which is typically smaller than that in dilute conditions, ζ depends on the dilute particle volume V_p; $\zeta = NV_p/V$, with N the number of microgels and V the accessible volume.

To obtain the collapsed size, we use that [2]

$$k = \frac{\zeta}{c} = \frac{\rho_s V_p}{m_{\text{pol}}} = \frac{\rho_s R_H^3}{\rho_{PNiPAM} R_{\text{col}}^3} \rightarrow R_{\text{col}} = R_H \left(\frac{\rho_s}{k \rho_{PNiPAM}} \right)^{1/3},$$
(1)

where m_{pol} is the polymer mass in a particle, ρ_s is the solvent density, $\rho_{PNiPAM} = 1.118$ g/cm^3 is the density of PNiPAM [22], and R_{col} is the collapsed radius. Recall that R_H is the hydrodynamic radius at the conditions where k is measured.

For $T = 30\,°C$ and pH = 7.5, in the absence of added salt, our ULC microgels have $k = 33 \pm 5$, and a collapsed radius $R_{\text{col}} = (150 \pm 10)$ nm.

Knowing R_{col} is important as we can use it to obtain the number of charges in one microgel particle [2]. From R_{col}, we find $m_{\text{pol}} = (4/3)\pi \rho_{PNiPAM} R_{\text{col}}^3$, and using the molecular weight of NiPAM and AAc, $M_{w,NiPAM} = 113$ g/mol and $M_{w,AAc} = 72$ g/mol, we determine the number of monomers in a microgel particle. Since we know that 5% of these momoners correspond to AAc groups, assuming all monomers reacted in the synthesis, we can then estimate the total number of potential charges per particle Q. We obtain $Q = (5.0 \pm 0.5) \times 10^6$.

We can check the validity of this estimate by obtaining R_{col} using the amount of bound water in the microgel. We know there is around 0.39g of bound water per gram of polymer [23], and that the most deswollen size we have measured, corresponding to high temperature and low pH, equals $R_H \approx 180$ nm [see Figs. 1(a) and 1(b)]. From this size, we estimate a collapsed radius of $R_{\text{col}} \approx R_H (1/1.39)^{1/3} \approx 160$ nm, consistent with what we found from viscometry and validating our estimate of Q. Knowing the number of potential charges in a microgel and its size allows estimating the number density of ions inside the particle at any of the considered T and pH.

So far, we have not considered salt concentration c_s as a means to change the microgel size. We consider this now, emphasizing that salt concentration provides an alternative way to achieve this without affecting, at least to leading order, the mixing between the polymer and the solvent; this allows deswelling to a size comparable to that we could alternatively have obtained by raising the temperature. We use NaCl in our experiments and progressively change its concentration at a constant pH of about (8.5 ± 0.5), where nearly all AAc is charged, and at two temperatures, $T = 40\,°C$ and $T = 60\,°C$, where the particles have, respectively, attained their maximum size or have appreciably deswollen to a bit more than half that size [see Fig. 1(b)]. We find that increasing c_s does not appreciably change the microgel size until the added salt concentration becomes comparable to the concentration of counterions inside the microgel [24]. Above this threshold, we find that $R_H \sim c_s^{-\beta}$, with $\beta = 1/5$; this is shown in Fig. 1(c) and is consistent with previously observed behavior in ionic microgels [24]. Note also that this scaling reflects that Q is constant, and thus that it does not appreciably change with particle size. This decrease in R_H could presumably continue to even higher c_s. However, as the particles progressively deswell with increasing c_s, van der Waals attractions between them also increase. In addition, since adding salt also screens the Yukawa-type electrostatic interaction between the microgels, these are no longer able to maintain colloidal stability, resulting in aggregation; the vertical lines in Fig. 1(c) indicate where aggregation is first detected at the two considered temperatures.

III. ANALYSIS OF THE SANS DATA

We perform neutron scattering experiments at the Oak Ridge National Laboratory (ORNL) Spallation Neutron Source (SNS) to investigate if there are changes in the internal structure of ULC microgels as they change size with
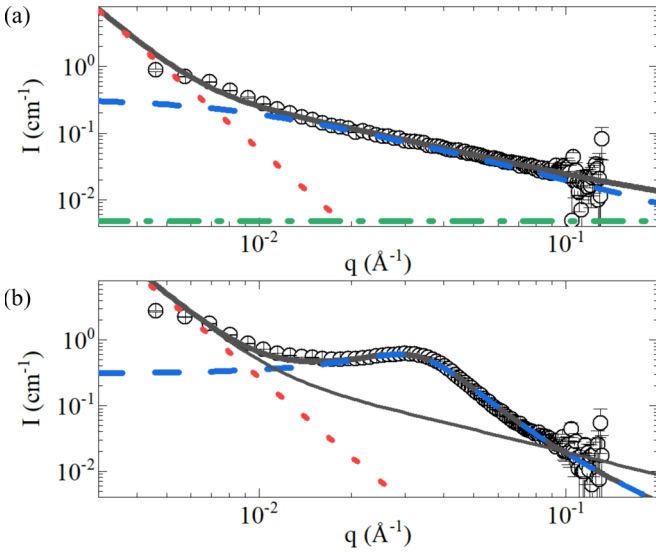
FIG. 2. (a) $P(q)$ for a dilute sample with $c_s = 0.5$ mM at $T = 40\,°$C. The thick solid line is a fit to Eq. (6). (b) $P(q)$ for a dilute sample with $c_s = 0.5$ mM at $T = 60\,°$C. The thick solid line is a fit to Eq. (8). The thin solid line is the best fit to Eq. (6), which clearly does not capture the presence of the peak. Dotted lines are the contribution from $P_2(q)$. Dashed lines are the contribution from $P_{LDB}(q)$ and $P_{BE}(q)$, respectively. The horizontal line in (a) is the contribution from incoherent scattering. In (b), this contribution is negligible compared to the other two.

temperature, pH, and salt concentration, and if there are, to quantify them. For details on the technique and data reduction refer to our Supplemental Material, Ref. [25], and to references therein. Ultimately, what one obtains is the scattering cross section per unit volume, which we will note as I, with the understanding that it would be in absolute units, cm^{-1} in our case, when indicated, and left in arbitrary units, arb. units, otherwise. Since we will not extract any information from the absolute value of I but only from its q-dependence, this difference is not significant.

To analyze the scattering data we consider that the form factor has three contributions:

$$P(q) = P_2(q) + P_1(q) + P_0(q). \quad (2)$$

Each of these can be traced back to a different origin. We will illustrate our model in detail by using scattering data for a dilute sample at pH $= 7.5$, $T = 40\,°$C, and $c_s = 0.5$ mM; see Fig. 2(a).

The term noted as $P_2(q)$ mostly contributes to the low-q region. Since we know that at the length scales accessible with light scattering, ULC microgels are well described as optically homogeneous and isotropic spheres [9], we use the corresponding form factor for this low-q contribution,

$$P_{HS}(q) = \left[3 \frac{\sin(qR) - qR\cos(qR)}{(qR)^3} \right]^2, \quad (3)$$

where R is the particle radius. However, since the low-q region of our SANS data corresponds to the high-q region of typical light scattering data, and also due to polydispersity, the characteristic minima in $P_{HS}(q)$ averages out, resulting in a $(qR)^{-4}$

limiting behavior. As a result, we take

$$P_2(q) = I_2 (qR)^{-4}, \quad (4)$$

where I_2 is the amplitude associated to this term. Its contribution to the scattering intensity of the example data plotted in Fig. 2(a) is shown in this figure with a dotted line.

The term $P_0(q)$ mostly contributes to I at high q. It is related to incoherent scattering and amounts to a constant background. Hence, $P_0(q) = I_b$. In Fig. 2(a) this contribution is shown with a horizontal dashed-dotted line.

The middle region of our SANS data corresponds to length scales within the ULC microgels, and therefore describes their internal structure. The q-dependence of I in this region exhibits the typical decay observed for many other microgel particles [16,26]; see Fig. 2(a). To model this contribution, we consider the typical internal structure of microgels, whose scattering is dominated by the correlations between polymer segments on the same chain [27,28]. The corresponding contribution to the form factor is given by the Lorentz-Debye-Bueche (LDB) model:

$$P_1(q) = P_{LDB}(q) = I_1 \frac{\Gamma(\mu)}{q\xi} \frac{\sin[\mu \arctan(q\xi)]}{[1 + (q\xi)^2]^{\mu/2}}, \quad (5)$$

where ξ is a correlation length associated with the blob or mesh size of the polymer network, $\mu = D_f - 1$, with D_f the fractal dimension of the chain, and Γ is the gamma function [9]. The quantity I_1 is the amplitude of this contribution.

There are three special cases of the LDB model, whereby it simplifies to other well-known models. For $\mu = 0$, corresponding to $D_f = 1$ and thus to straight polymer chains, $P_{LDB}(q) = \arctan(q\xi)/(q\xi)$. For $\mu = 1$, corresponding to $D_f = 2$ and thus to a random-walk chain, the LDB model becomes a Lorentzian term [28]: $P_{LDB}(q) = 1/[1 + (q\xi)^2]$. Finally, for $\mu = 2$, corresponding to $D_f = 3$ and thus to a space filling chain, we obtain that $P_{LDB}(q) = 1/[1 + (q\xi)^2]^2$; the LDB model becomes a Debye-Bueche term. The LDB contribution to the scattering intensity of the example data considered in Fig. 2(a) is shown in this figure with a dashed line.

Incorporating all of the components into Eq. (2), we have

$$P(q) = I_2(qR)^{-4} + I_1 \frac{\Gamma(\mu)}{q\xi} \frac{\sin[\mu \arctan(q\xi)]}{[1 + (q\xi)^2]^{\mu/2}} + I_b, \quad (6)$$

which fits our data well, as shown with a solid line in Fig. 2(a). Note that the q range of our data mostly focuses on intermediate q values, where $P_1(q) = P_{LDB}(q)$ is the dominant contribution to I. In our fit, R is set to the hydrodynamic radius obtained in DLS; hence, $R = R_H = 7000$ Å. This is justified given that ULC microgels are very homogeneous spheres when probed on length scales accessible with visible light [10,11]. The only fitting parameters then are μ and ξ. We find $\mu = 0.2$ and $\xi = 150$ Å for the data plotted in Fig. 2(a). The low value of μ comes from the open structure of the microgels at pH $= 7.5$ and $T = 40\,°$C, corresponding to a swollen particle. The rather large value of ξ again points out to a swollen particle where we expect a large blob size.

The LDB model, however, does not work for all of our data. In some cases we observe a scattering intensity like that in Fig. 2(b), where the sample is a dilute microgel suspension at pH $= 7.5$ and $c_s = 0.5$ mM, but at $T = 60\,°$C. The most

notable feature in this case is the presence of a peak in I at intermediate q. Note the LDB model is unable to describe the data, as shown by the thin solid line in Fig. 2(b), which is the best fit of the data with Eq. (6). The appearance of the observed peak indicates that a new relevant length scale emerges inside the particles. For the case of both macrogels [29–31] and ULC microgels [9], this length scale was attributed to the occurrence of internal microphase separation where solvent-poor and solvent-rich regions coexist, as described by the theory of Borue and Erukhimovich (BE) [30,32]. In this case, we take

$$P_1(q) = P_{BE}(q) = I_1 \left[(r_0 q)^2 + t + \frac{1}{s + (r_0 q)^2} \right]^{-1}, \quad (7)$$

where r_0 is a length scale associated with the correlations of the fixed charges in the polymer network, t is a dimensionless solvent quality, and $s = (r_0/\kappa^{-1})^2$, with κ^{-1} the Debye screening length. Combining this $P_1(q)$ with the low- and high-q contributions gives

$$P(q) = I_2(qR)^{-4} + I_1 \left[(r_0 q)^2 + t + \frac{1}{s + (r_0 q)^2} \right]^{-1} + I_b. \quad (8)$$

This model correctly describes the data in Fig. 2(b), as shown by the thick solid line in this figure; the BE contribution is also shown with a dashed line. In particular, the model correctly reproduces the observed peak. Here, consistent with what we did with the data at $T = 40\,°C$, we set $R = R_H = 3800$ Å, and leave r_0, s and t as fitting parameters. From the fit, we obtain $r_0 = 17$ Å, $s = 0.8$, and $t = -1.2$. Note $t < 0$, indicating the solvent quality is poor and consistent with $T > T_{LCST}$. Note also $s < 1$, but close to 1, indicating that both screening due to fixed-charge correlations as well as due to the ions is relevant and contribute to the electrostatic contributions to the free energy. Indeed, from r_0 and s, we obtain $\kappa^{-1} = 20$ Å, which is nearly identical to r_0. This value of κ^{-1} compares well with the estimate based on Q and R_H: $\kappa^{-1} = \sqrt{\frac{R_H^3}{3 l_B Q}} \approx 25$ Å, with l_B the Bjerrum length. Importantly, the obtained values of s and t approximately lie on the spinodal line, in the context of BE theory, associated with microphase separation. It is thus the competition between a strong tendency to demix at $t < 0$, and the swelling-favored due to electrostatic/ionic effects that ultimately bring the gel into a microphase separated state where solvent-poor and solvent-rich regions coexist. We emphasize the ULC microgels do not experience macrophase but microphase separation. There are thus internal inhomogeneities, but these are small; hence on length scales accessible with light scattering, ULC microgels appear as optically homogenous spheres, as reported before [9].

We can also independently estimate r_0 from the network parameters. We know that in a poor solvent [29,30,32], which is our case,

$$r_0 = a_m \left(\frac{48 \pi l_B}{a_m} \phi_p \alpha^2 \right)^{-1/4} \quad (9)$$

with a_m the size of a monomer, ϕ_p the volume fraction of the polymer in the microgel, and α the degree of ionization. For NiPAM, $a_m \approx 2.5$ Å. In addition, the volume fraction of the
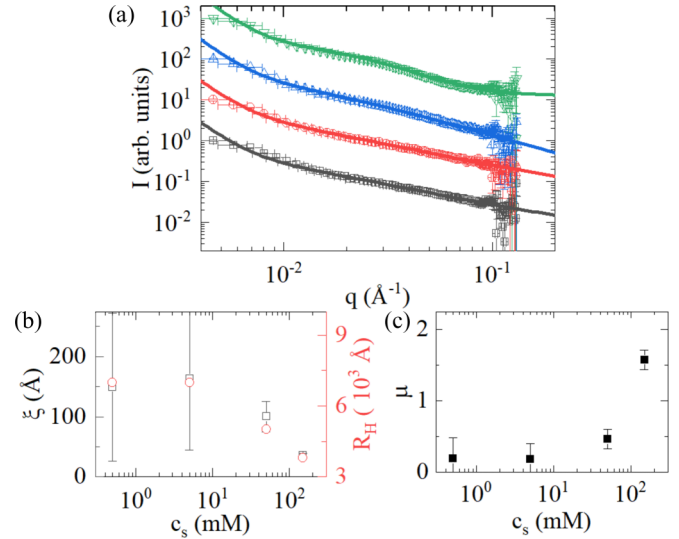

FIG. 3. (a) $P(q)$ for dilute microgel suspensions for $c_s = 0.5$ mM (squares), 5 mM (circles), 50 mM (up triangles), and 150 mM (down triangles), at $T = 40\,°C$ and pH = 7.5. The lines are fits to Eq. (6). (b) The blob size ξ (squares) obtained from the fits in (a) versus salt concentration. R is taken as the dilute hydrodynamic radius measured with DLS in Fig. 1(c). (c) The parameter $\mu = D_f - 1$ obtained from the fits in (a) versus salt concentration.

polymer in the microgel can be obtained from the ratio of the swollen-to-collapsed sizes, $\phi_p = (R_{col}/R_H)^3$. Using that $\alpha = Q/N_m \approx 0.05$, where N_m is the total number of monomers, and that we have estimates for all other parameters in Eq. (13) at pH = 7.5 and $T = 60\,°C$, we find $r_0 \approx 5$ Å, which is of the same order as the value obtained from the fit.

Note we have not discussed the structure factor $S(q)$ of the colloidal suspension. This is because the minimum qR_H value in our experiments, corresponding to the smallest particle radius of our ULC microgels and smallest q, is about 10^3. In this case, we can safely assume $S(q) = 1$. The q-dependence of I is thus exactly that of $P(q)$.

IV. RESULTS

A. Low ζ, pH = 7.5, $T = 40\,°C$

For dilute suspensions at $T = 40\,°C$, the form factor is well fitted by Eq. (6) at all salt concentrations; see Fig. 3(a). From the fits, we find that ξ monotonically decreases with increasing c_s. Remarkably, this behavior tracks the behavior of R_H, as shown in Fig. 3(b), indicating that the particles are shrinking uniformly [33]. Concomitantly, μ monotonically increases, as shown in Fig. 3(c); this is consistent with the ULC microgels becoming denser with shrinking and thus with the polymer chains progressively filling more of the available space.

B. Low ζ, pH = 7.5, $T = 60\,°C$

At higher T, we can no longer fit the middle and most significant q region of I using the LDB model, as indicated before. This is due to the emergence of a peak in I [see Fig. 4(a)], which we associate with a new internal length scale due to microphase separation. Hence, instead of the LDB model, we
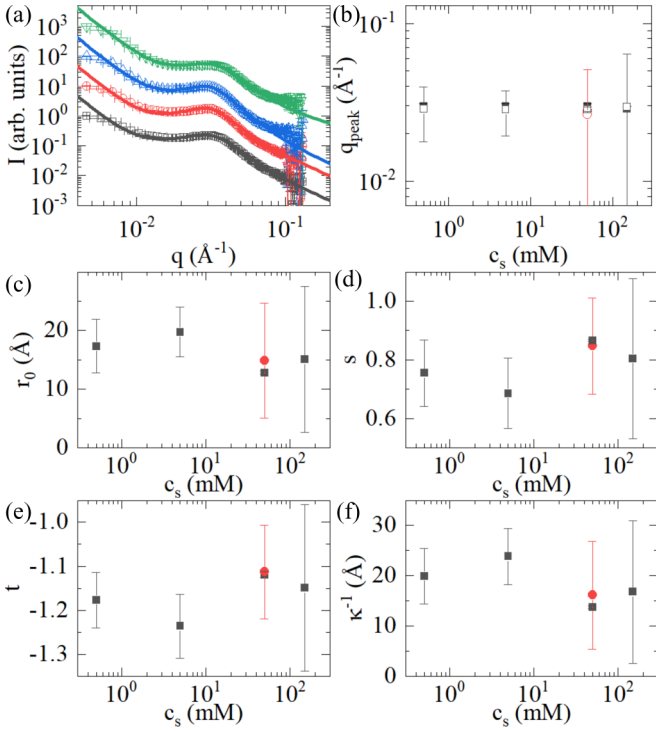
FIG. 4. (a) $P(q)$ for dilute microgel suspensions for $c_s =$ 0.5 mM, 5 mM, 50 mM, and 150 mM, at $T = 60\,^{\circ}\text{C}$ and pH $= 7.5$. The lines are fits to Eq. (8). The BE parameters are shown as a function of salt concentration: (c) r_0, (d) s, and (e) t. (b) Peak position measured in (a) (closed symbols) and calculated values from the fitting parameters using Eq. (10) (open symbols). (f) κ^{-1} calculated from the fitting parameters. In (b)–(f), the circle data point is at $T = 50\,^{\circ}\text{C}$.

use the BE model. The fits to the data can be seen as the lines in Fig. 4(a). We find the peak remains at an essentially fixed q of $q_{peak} = (0.030 \pm 0.001)$ Å^{-1}; see Fig. 4(b). Furthermore, regardless of salt concentration, the fitting parameters do not significantly change; we find $r_0 \approx 15$ Å, as shown in Fig. 4(c), $s \approx 0.8$, as shown in Fig. 4(d), and $t \approx -1.2$, as shown in Fig. 4(e). As mentioned before, the negative value of t indicates the demixing desire at high T, while a value of $s < 1$, but close to 1, reflects that we lie within the phase separation region expected in BE theory, whereby the effect of both ionic and fixed-charge contributions compete with the effect of T.

Note that at $T = 40\,^{\circ}\text{C}$, adding salt results in a size similar to that obtained at $T = 60\,^{\circ}\text{C}$ without salt [see Fig. 1(c)]. In the first case, there is no peak in the SANS data, while at $T = 60\,^{\circ}\text{C}$, we always find a peak in the data regardless of salt concentration. This indicates that change in the particle size alone is not enough to cause internal microphase separation inside the ULC microgels. The demixing at high temperature is a requirement for this to occur. In this case, this contribution to the free energy, which favors shrinking, competes with electrostatic and ionic effects, which favors swelling. The result of this competition is internal microphase separation and a dramatic change in internal structure, with solvent-rich and solvent-poor regions within the particles. At $T = 40\,^{\circ}\text{C}$, even for comparable sizes to those where we see microphase separation, this competition between demixing and electrostatic and ionic effects completely disappears.

From s and r_0 we can calculate κ^{-1}. We find that κ^{-1} slightly decreases with c_s, but not significantly considering the error associated with our calculations; see Fig. 4(f). Since $\kappa^{-1} \sim R_H^{3/2}$ and R_H changes by a factor of 2 between $c_s =$ 0.5 mM and $c_s = 150$ mM, we expect κ^{-1} to decrease by a factor of $\sim$2.8, which is within what we find experimentally.

In addition, in BE theory the position of the peak is related to the two electrostatic-related length scales, r_0 and κ^{-1}. Specifically,

$$q_{peak} = \sqrt{\left(\frac{1}{r_0}\right)^2 - \left(\frac{1}{\kappa^{-1}}\right)^2}. \quad (10)$$

Using the fit results, we see that the calculated peak positions agree with those found experimentally, as shown in Fig. 4(b).

C. Changing ζ, no salt

Another way to potentially change the size of the ULC microgels is to increase the generalized packing fraction ζ. One of the mechanisms that can cause shrinking in this way is counterion-induced osmotic deswelling [6,34]. The key players in this mechanism are the free ions that are able to leave the microgel. As the actual volume fraction ϕ increases, the available volume outside of the microgel particles decreases, causing an increase in the osmotic pressure of the ions, which eventually causes shrinking of the microgels. The fraction of deconfined ions can be estimated as [6]

$$\gamma = \frac{(\kappa^{-1} + R_H)^3 - R_H^3}{R_H^3} \approx 3\kappa^{-1}/R_H. \quad (11)$$

Since κ^{-1} depends on Q, which is constant, and on R_H, γ is essentially determined by the particle size alone. At $T = 40\,^{\circ}\text{C}$, pH $= 7.5$ and small c_s, we have $R_H = 7000$ Å, resulting in $\gamma = 0.01$. Similarly, at $T = 60\,^{\circ}\text{C}$, pH $= 7.5$ and small c_s, the microgel radius is $R_H = 3800$ Å, and we obtain $\gamma = 0.02$. To estimate the osmotic pressure of these ions, we treat them as an ideal gas; the associated osmotic pressure is then given by

$$\pi_c(\phi) = k_B T \frac{\gamma Q}{V_p} \frac{\phi}{1 - \phi}. \quad (12)$$

Since at low ζ and $T = 40\,^{\circ}\text{C}$, the shrinking behavior is uniform, we assume this is still the case and allow R_H to track the blob size ξ. Using this assumption, we can describe our data; see Fig. 5(a). In this case, only ξ, μ, and the amplitudes of the three contributions to I are left as fitting parameters. From the fits, we find that ξ is approximately constant up to $\zeta \simeq 0.75$, after which it decreases; see Fig. 5(b). This decrease happens approximately when π_c begins to appreciably increase, consistent with possible counterion-induced deswelling. Note, however, that while our results are consistent with counterion-induced shrinking, we cannot directly confirm this with our SANS data, since we do not have data at sufficiently low q for us to obtain a meaningful independent estimate of R_H. Furthermore, consistent with shrinking and densifying, μ also increases with ζ for $\zeta > 0.75$; see Fig. 5(c).

When the temperature is increased to $T = 60\,^{\circ}\text{C}$, the competition between demixing and electrostatic/ionic effects causes a peak to appear in I; see Fig. 5(d). This is consistent with what we find at low ζ. The data are well described by
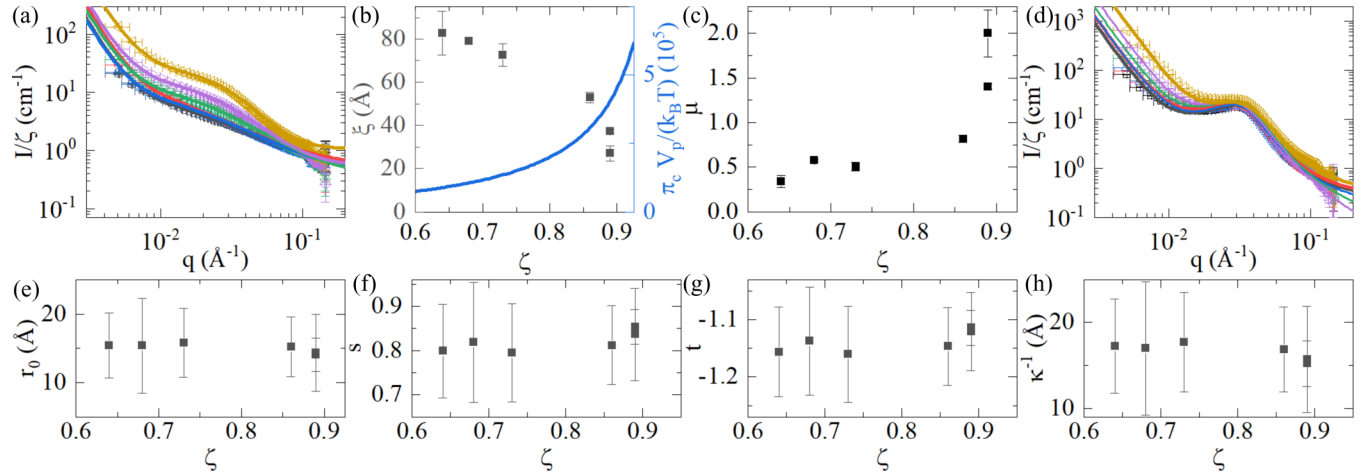
FIG. 5. (a) $P(q)$ for salt-free samples at $T = 40\,°C$ and $pH = 7.5$ with increasing ζ: $\zeta = 0.64$ (squares), 0.68 (circles), 0.73 (up triangles), 0.86 (down triangles), and 0.89 (diamonds and left triangles). Lines are fits to Eq. (6). (b) Blob size ξ obtained from the fits in (a) versus ζ. The values of $R = R_H$ have been taken assuming uniform shrinking with ζ. The osmotic pressure from Eq. (12), taking $\phi = \zeta$, is shown as a solid line. (c) Fitting parameter μ versus ζ. (d) $P(q)$ for samples at $T = 60\,°C$ and at the same ζ indicated in (a). Lines are fits to Eq. (8). The fit parameters are r_0 (e), s (f), and t (g). (h) κ^{-1} calculated from r_0 and s.

Eq. (8) with fitting parameters consistent with those in dilute conditions; see Figs. 5(e)–5(h). Even if there is counterion-induced deswelling, the internal length scales are determined by microphase separation and are not related to the microgel size.

D. Changing ζ, $c_s = 150$ mM

Increasing the salt concentration to a high value is known to eliminate counterion-induced deswelling [35]. Consistent with this, we find that the q-dependence of I does not appreciably change with ζ. Samples at the same T but with different ζ provide almost identically-scaling I curves, as shown by the overlaid data in Fig. 6. Below a critical temperature, the ULC microgels do not demix internally, but once this threshold is reached, a pronounced shoulder appears in I. The approach to

this critical demixing temperature can be seen in the increasing value of μ and decreasing value of ξ in the vicinity of this temperature; see Figs. 7(a) and 7(b). Note that at $T \approx 40\,°C$ at this high c_s, both the LDB and BE models are able to describe

FIG. 7. Fitting parameters for the fits in Fig. 6 with varying ζ: $\zeta = 0.01$ (squares), 0.3 (circles), 0.5 (up triangles), 0.7 (down triangles), and 1.0 (diamonds). (a, b) Fitting parameters for fits to Eq. (6) of $P(q)$ at varying T and ζ: μ versus T in (a) and ξ and R_H versus T in (b). (c–e) Fitting parameters for fits to Eq. (8) of $P(q)$ at varying T and ζ: r_0 versus T in (c), s versus T in (d), and t versus T in (e). (f) The screening Debye length calculated from r_0 and s. Fits were done at $T = 37\,°C$, $40\,°C$, and $43\,°C$ to both Eq. (6) and Eq. (8) to show the transition between the two distinct regimes.
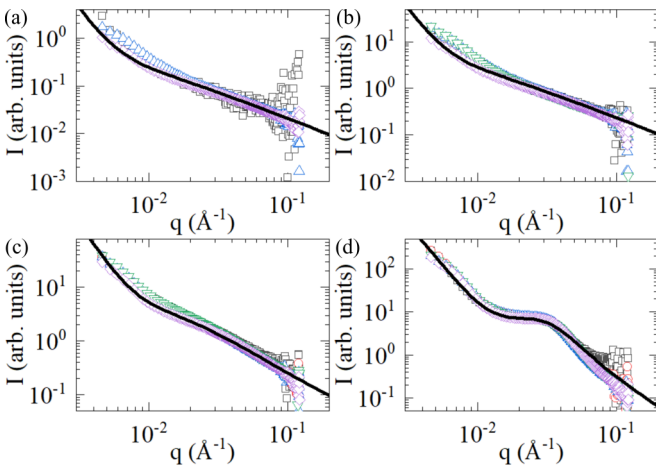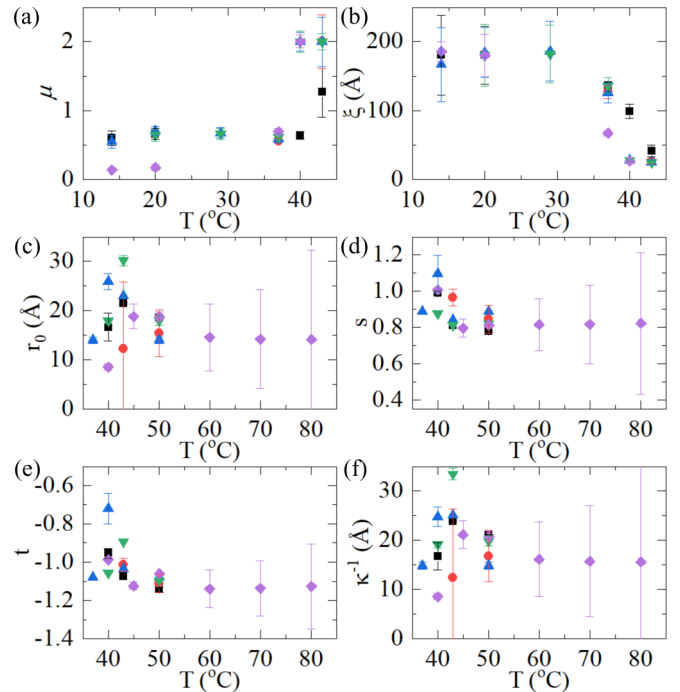

FIG. 6. $P(q)$ for samples with varying ζ: $\zeta = 0.01$ (squares), 0.3 (circles), 0.5 (up triangles), 0.7 (down triangles), and 1.0 (diamonds). The four temperatures shown are $T = 14\,°C$ (a), $20\,°C$ (b), $37\,°C$ (c), and $50\,°C$ (d). Lines in (a)–(c) are fits to Eq. (6). In (d) the line is a fit to Eq. (8).

the data, reflecting that it is around this temperature when demixing becomes significant relative to electrostatic/ionic effects. In this case, the relevant internal length scales in either model, ξ and r_0, approximately agree with each other; see Figs. 7(b) and 7(c). At higher T, the values of s and t obtained from the fits agree with our prior findings; see Figs. 7(d) and 7(e). This is also the case for κ^{-1}; see Fig. 7(f).

V. CONCLUSION

We have shown that the competition between demixing at high T and the swollen-favored situation due to electrostatic and ionic effects can result in nonuniform behavior and internal microphase separation of PNiPAM ULC microgels. This is clearly reflected in the presence of a scattering peak at associated length scales that are well within the particles. The resultant scenario is well captured by BE theory, which is parametrized in terms of a dimensionless solvency parameter t, which is negative for our ULC microgels, indicative of demixing, and a dimensionless screening length s that weighs the relative importance of screening due to correlations between fixed charges and screening due to the ions; our results indicate that s is close to 1, suggesting that both effects play a relevant role for our ULC microgels. In addition, $s < 1$ and $|s - t| \approx 2$, indicating, according to BE theory, occurrence of microphase separation inside the particles.

In contrast, at lower T, where demixing is not as relevant, the behavior is uniform and the internal mesh size tracks the behavior of the hydrodynamic radius of the particles. Hence, it is not size *per se* that triggers internal microphase separation, but rather the competition between demixing and electrostatic/ionic effects.

Similar conclusions are reached regardless of ζ; here also, we find that for charged microgels like ours, T is the governing parameter that determines whether or not there is internal microphase separation. At low T and in the presence of counterion-induced deswelling, the behavior is consistent with uniform deswelling. In contrast, at high T, internal microphase separation, as captured by BE theory, occurs, reflecting nonuniform behavior.

Overall, our results indicate that one should be careful when assuming that microgel deswelling is uniform throughout the particle; depending on the conditions and of the type of microgel, this assumption may be a gross oversimplification of how the internal structure of these compressible particles changes as their size is modified.

[1] A. Fernandez-Nieves, H. Wyss, J. Mattsson, and D. A. Weitz, *Microgel Suspensions: Fundamentals and Applications* (Wiley-VCH Verlag and Co., Weinheim, Germany, 2011).

[2] A. Scotti, U. Gasser, E. S. Herman, M. Pelaez-Fernandez, J. Han, A. Menzel, L. A. Lyon, and A. Fernández-Nieves, Proc. Natl. Acad. Sci. USA **113**, 5576 (2016).

[3] A. Scotti, A. R. Denton, B. Monia, A. R. Houston, R. Schweins, I. I. Potemkin, and W. Richtering, Macromolecules **52**, 3995 (2019).

[4] I. B. de Aguiar, T. van de Laar, M. Meireles, A. Bouchoux, J. Sprakel, and K. Schroen, Sci. Rep. **7**, 10223 (2017).

[5] N. Gnan and E. Zaccarelli, Nat. Phys. **15**, 683 (2019).

[6] R. Borrega, M. Cloitre, I. Betremieux, B. Ernst, and L. Leibler, Europhys. Lett. **47**, 729 (1999).

[7] M. Cloitre, R. Borrega, F. Monti, and L. Leibler, C. R. Physique **4**, 221 (2003).

[8] M. Urich and A. R. Denton, Soft Matter **12**, 9086 (2016).

[9] J. S. Hyatt, A. M. Douglas, C. Stanley, C. Do, T. H. Barker, and A. Fernández-Nieves, Phys. Rev. E **95**, 012608 (2017).

[10] H. Bachman, A. C. Brown, K. C. Clarke, K. S. Dhada, A. Douglas, C. E. Hansen, E. Herman, J. S. Hyatt, P. Kodlekere, Z. Meng, *et al.*, Soft Matter **11**, 2018 (2015).

[11] M. Brugnoni, A. C. Nickel, L. C. Kröger, A. Scotti, A. Pich, K. Leonhard, and W. Richtering, Polymer Chem. **10**, 2397 (2019).

[12] A. C. Brown, S. E. Stabenfeldt, B. Ahn, R. T. Hannan, K. S. Dhada, E. S. Herman, V. Stefanelli, N. Guzzetta, A. Alexeev, and W. A. Lam, Nat. Mater. **13**, 1108 (2014).

[13] J. Gao and B. J. Frisken, Langmuir **19**, 5217 (2003).

[14] J. Gao and B. J. Frisken, Langmuir **19**, 5212 (2003).

[15] T. Hoare and D. McLean, J. Phys. Chem. B **110**, 20327 (2006).

[16] A. F. Routh and W. B. Zimmerman, J. Colloid Interface Sci. **261**, 547 (2003).

[17] W. Brown, *Dynamic Light Scattering: The Method and Some Applications* (Oxford University Press, New York, 1993).

[18] J. S. Hyatt, C. Do, X. Hu, H. S. Choi, J. W. Kim, L. A. Lyon, and A. Fernandez-Nieves, Phys. Rev. E **92**, 030302(R) (2015).

[19] A. Einstein, Ann. Phys. **322**, 549 (1905).

[20] A. Einstein, Ann. Phys. **339**, 591 (1911).

[21] G. K. Batchelor, J. Fluid Mech. **83**, 97 (1977).

[22] H. G. Schild, Prog. Polym. Sci. **17**, 163 (1992).

[23] A. K. Lele, M. M. Hirve, M. V. Badiger, and R. A. Mashelkar, Macromolecules **30**, 157 (1997).

[24] A. Fernandez-Nieves, A. Fernandez-Barbero, and F. J. de las Nieves, J. Chem. Phys. **115**, 7644 (2001).

[25] See Supplemental Material at http://link.aps.org/supplemental/10.1103/PhysRevE.103.022614 for details on SANS.

[26] J. K. Dhont, *An Introduction to Dynamics of Colloids* (Elsevier, Amsterdam, The Netherlands, 1996).

[27] W. D. Dozier, J. S. Huang, and L. J. Fetters, Macromolecules **24**, 2810 (1991).

[28] P.-G. de Gennes, *Scaling Concepts in Polymer Physics* (Cornell University Press, Ithaca, NY, 1979).

[29] M. Shibayama, T. Tanaka, and C. C. Han, J. Chem. Phys. **97**, 6829 (1992).

[30] M. Shibayama, T. Tanaka, and C. C. Han, J. Chem. Phys. **97**, 6842 (1992).

[31] F. Ikkai and M. Shibayama, Polymer **48**, 2387 (2007).

[32] V. Y. Borue and I. Y. Erukhimovich, Macromolecules **21**, 3240 (1988).

[33] Note this behavior has often been described as affine. Strictly speaking, however, the transformation is not affine, it is uniform. Affine transformations preserve parallel lines, which would require μ to be constant as our microgels deswell. Shrinking, even when ξ is proportional to R_H, implies changes in the polymer configuration that invalidate the otherwise correct reference to affinitiy.

[34] M. Pelaez-Fernandez, A. Souslov, L. A. A. Lyon, P. M. M. Goldbart, and A. Fernández-Nieves, Phys. Rev. Lett. **114**, 098303 (2015).

[35] U. Gasser, A. Scotti, and A. Fernandez-Nieves, Phys. Rev. E **99**, 042602 (2019).